Inorg. Chem. **2003**, *42*, 679–688

Electronic Structure Contributions to Electron-Transfer Reactivity in Iron–Sulfur Active Sites: 1. Photoelectron Spectroscopic Determination of Electronic Relaxation

Pierre Kennepohl and Edward I. Solomon*

Department of Chemistry, Stanford University, Stanford, California 94305-5080

Received May 8, 2002

Electronic relaxation, the change in molecular electronic structure as a response to oxidation, is investigated in $[FeX_4]^{2-,1-}$ (X = Cl, SR) model complexes. Photoelectron spectroscopy, in conjunction with density functional methods, is used to define and evaluate the core and valence electronic relaxation upon ionization of $[FeX_4]^{2-}$. The presence of intense yet formally forbidden charge-transfer satellite peaks in the PES data is a direct reflection of electronic relaxation. The phenomenon is evaluated as a function of charge redistribution at the metal center (Δq_{rlx}) resulting from changes in the electronic structure. This charge redistribution is calculated from experimental core and valence PES data using a valence bond configuration interaction (VBCI) model. It is found that electronic relaxation is very large for both core (Fe 2p) and valence (Fe 3d) ionization processes and that it is greater in $[Fe(SR)_4]^{2-}$ than in $[FeCl_4]^{2-}$. Similar results are obtained from DFT calculations. The results suggest that, although the lowest-energy valence ionization (from the redox-active molecular orbital) is metal-based, electronic relaxation causes a dramatic redistribution of electron density ($\sim$0.7$\bar{e}$) from the ligands to the metal center corresponding to a generalized increase in covalency over all M–L bonds. The more covalent tetrathiolate achieves a larger Δq_{rlx} because the LMCT states responsible for relaxation are significantly lower in energy than those in the tetrachloride. The large observed electronic relaxation can make significant contributions to the thermodynamics and kinetics of electron transfer in inorganic systems.

Introduction

Electron-transfer processes are of fundamental importance in many key areas of chemistry.[1−10] In biological systems, effective control of electrons is paramount in many of the most important biochemical reaction pathways.[1] The control of biological electron flux is achieved in vivo through the presence of electron-transfer and -transport (ET) proteins, often containing transition metal redox centers. The elucidation of the factors that control chemical and biochemical functionality of such redox sites has attracted significant attention in the bioinorganic community. A critical issue is to define effectively the electronic structure contributions to the redox properties of the active sites in these ET proteins.

An important class of ET active sites is the so-called iron−sulfur (FeS) active sites, such as those found in rubredoxins (Rds) and ferredoxins (Fds). Rds have the simplest of the FeS active sites: a single high-spin iron center coordinated to the protein through four cysteinate residues. The biologically relevant redox couple involves the Fe^{II} (reduced) and Fe^{III} (oxidized) redox states. The $[Fe(SR)_4]^{2-,1-}$ active sites in Rds and model systems have received significant attention in recent years.[11−18] Spectroscopy on more general $[FeX_4]^{2-,1-}$ model systems has also provided insight into certain aspects

* Correspondence should be addressed to this author. Electronic-mail communication is encouraged (edward.solomon@stanford.edu).

(1) Holm, R. H.; Kennepohl, P.; Solomon, E. I. *Chem. Rev.* **1996**, *96*, 2239−2314.
(2) Bellelli, A.; Brunori, M.; Brzezinski, P.; Wilson, M. T. *Methods (San Diego)* **2001**, *24*, 139−152.
(3) Moser, C. C.; Page, C. C.; Chen, X.; Dutton, P. L. *Subcell. Biochem.* **2000**, *35*, 1−28.
(4) Kuznetsov, A. M.; Ulstrup, J. *Electrochim. Acta* **2000**, *45*, 2339−2361.
(5) Brunschwig, B. S.; Sutin, N. *Coord. Chem. Rev.* **1999**, *187*, 233−254.
(6) Skourtis, S. S.; Beratan, D. N. *Adv. Chem. Phys.* **1999**, *106*, 377−452.
(7) Mataga, N.; Miyasaka, H. *Adv. Chem. Phys.* **1999**, *107*, 431−496.
(8) Utimoto, K. *New Challenges Org. Electrochem.* **1998**, 279−306.
(9) Marcus, R. A. *J. Electroanal. Chem.* **1997**, *438*, 251−260.
(10) Barbara, P. F.; Meyer, T. J.; Ratner, M. A. *J. Phys. Chem.* **1996**, *100*, 13148−13168.
(11) Im, S. G.; Sykes, A. G. *J. Chem. Soc., Dalton Trans.* **1996**, 2219−2222.

10.1021/ic020330f CCC: $25.00
Published on Web 01/16/2003

of the chemical properties of these sites,[19−21] but the elucidation of electronic structure contributions to their redox chemistry has not yet been fully achieved.

Variable-photon-energy photoelectron spectroscopic (VEPES) studies of the $[FeCl_4]^{2-,1-}$ redox couple have provided important insights into the electronic structures of the reduced and oxidized forms of $[FeX_4]$ redox sites.[19−21] Importantly, a very large change in the electronic structure was observed between $[FeCl_4]^{2-}$ and $[FeCl_4]^{1-}$: although the reduced form exhibits a rather "normal" electronic structure, the oxidized species was shown to have an unusual "inverted" bonding scheme, where the filled metal 3d manifold is at deeper binding energy than the ligand valence manifold.[19] This change in electronic structure derives from differences in repulsion of metal-based electrons in the two redox states. The study concluded by emphasizing that a large change in the electronic structure occurs upon redox and by suggesting that such pronounced electronic relaxation upon ionization might be important in defining the redox properties of these and similar active sites. Earlier theoretical studies on simple $[Fe(SR)_4]^{2-,1-}$ redox centers also pointed to some very interesting redox behavior, suggesting that the redox process was best described as a ligand-based process.[22,23] This possibility was never fully investigated from an experimental perspective. To address issues relating to function properly, it is necessary to develop a self-consistent description of the electronic structure in both oxidation states and define the electronic structure changes that occur in the redox process.

This present study experimentally defines electronic relaxation and provides the foundation for two further studies focusing on the detailed evaluation of electronic structure contributions to the redox thermodynamics (part 2) and electron-transfer kinetics (part 3) of $[Fe(SR)_4]^{2-,1-}$ and related actives sites.[24,25] Using results from core and valence ionization spectroscopy on the ferrous species, we define a mechanism by which changes in the electronic wave function, i.e., electronic relaxation, can be observed and quantified. The overall effect of electronic relaxation is observable as the change in the electron density at the metal center (Δq_{rlx}) that is attributed to changes in the electronic wave function in response to oxidation of the reduced species. To determine Δq_{rlx}, a valence bond configuration interaction (VBCI) model is used to properly define an unrelaxed reference state, termed the Koopmans state, from which electronic relaxation is calculated. Contributions to Δq_{rlx} are evaluated explicitly using the VBCI model, as well as density functional theory (DFT) methods to determine the origin of the phenomenon from a molecular orbital (MO) perspective. Results from the experimental and theoretical models are compared, providing the groundwork for an assessment of the importance and influence of Δq_{rlx} on the redox properties of $[FeX_4]^{2-,1-}$. These methods are applied to determine differences on electronic relaxation between the redox couples.

Experimental Section

Photoelectron Spectroscopy. Spectroscopic data were obtained on three different instruments: a Perkin-Elmer PHI system employing synchrotron radiation from the Stanford Synchrotron Radiation Laboratory (SSRL) at BL 10-1 (core) and 1-2 (valence), a Vacuum Generators ESCALAB Mk II, and a VG Instruments M-Probe, each using a conventional Al Kα (1486.6 eV) anode. Variable-photon-energy data were obtained at SSRL using the ion-pumped PHI chamber equipped with a double-pass cylindrical mirror analyzer operating at a pass energy of 25 eV; data were collected with a base pressure of $<2 \times 10^{-10}$ Torr in the analytic chamber. Specific SSRL beamline characteristics have been described elsewhere.[26] Conventional radiation sources (ESCALAB and M-Probe) were used for core-level data collection using a hemispherical analyzer operating at a pass energy of 20 eV; the analyzer chamber was maintained at $<5 \times 10^{-10}$ Torr. All data were signal-averaged until the signal-to-noise ratio was >20; sample integrity was internally verified by comparison of initial and final scans. Synchrotron data were normalized to the incident flux by monitoring the photoelectron signal from a gold-coated stainless steel mesh located in the path of the monochromatized radiation. All data were obtained at spectroscopic energy resolutions of ≤0.25 eV.

Samples were prepared and mounted as fine powders onto a sample plate using either Ga or conductive carbon substrate; all samples were mounted under N_2 or Ar atmosphere with <2 ppm of O_2 and transferred directly to the UHV environment. $[N(CH_2CH_3)_4]_2[Fe(X)_4]$ (where X = Cl, SPh) samples were prepared and recrystallized using literature methods.[27,28] Sample charging was compensated by using an electron flood gun at minimum energy and current settings for stable and undistorted data. Core binding energies were referenced to the strong background C 1s signal (285.0 eV). Valence binding energies were referenced and indexed using three independent methods: internal calibration using counterion peaks and external calibration using Ga (when used as substrate) and/or Au (from submonolayer Au sputtering onto the sample surface). Referenced data obtained from all three calibration methods gave results that were identical within the experimental resolution of the data. Sample integrity was verified by EPR of the irradiated sample, which indicated no observable deterioration over the course of data acquisition. Other tetrathiolate models, such as

(12) Jensen, T. J.; Gray, H. B.; Ulstrup, J. *J. Inorg. Biochem.* **1999**, *74*, 181−181.
(13) Kummerle, R.; ZhuangJackson, H.; Gaillard, J.; Moulis, J. M. *Biochemistry* **1997**, *36*, 15983−15991.
(14) Kummerle, R.; Kyritsis, P.; Gaillard, J.; Moulis, J. M. *J. Inorg. Biochem.* **2000**, *79*, 83−91.
(15) Moreno, C.; Franco, R.; Moura, I.; Legall, J.; Moura, J. J. G. *Eur. J. Biochem.* **1993**, *217*, 981−989.
(16) Ayhan, M.; Xiao, Z. G.; Lavery, M. J.; Hammer, A. M.; Scrofani, S. D. B.; Wedd, A. G. *ACS Symp. Ser.* **1996**, *653*, 40−56.
(17) dePelichy, L. D. G.; Smith, E. T. *Biochemistry* **1999**, *38*, 7874−7880.
(18) Moulis, J. M. *Theor. Chem. Acc.* **1999**, *101*, 223−227.
(19) Butcher, K. D.; Didziulis, S. V.; Briat, B.; Solomon, E. I. *J. Am. Chem. Soc.* **1990**, *112*, 2231−2242.
(20) Butcher, K. D.; Didziulis, S. V.; Briat, B.; Solomon, E. I. *Inorg. Chem.* **1990**, *29*, 1626−1637.
(21) Butcher, K. D.; Gebhard, M. S.; Solomon, E. I. *Inorg. Chem.* **1990**, *29*, 2067−2074.
(22) Noodleman, L.; Norman, J. G.; Osborne, J. H.; Aizman, A.; Case, D. A. *J. Am. Chem. Soc.* **1985**, *107*, 3418−3426.
(23) Norman, J. G.; Jackels, S. C. *J. Am. Chem. Soc.* **1975**, *97*, 3833−3835.
(24) Kennepohl, P.; Solomon, E. I. *Inorg. Chem.* **2003**, *42*, 689−695.
(25) Kennepohl, P.; Solomon, E. I. *Inorg. Chem.* **2003**, *42*, 696−708.
(26) Guckert, J. A.; Lowery, M. D.; Solomon, E. I. *J. Am. Chem. Soc.* **1995**, *117*, 2817−2844.
(27) Lauher, J. W.; Ibers, J. A. *Inorg. Chem.* **1975**, *14*, 348−352.
(28) Koch, S. A.; Maelia, L. E.; Millar, M. *J. Am. Chem. Soc.* **1983**, *105*, 5944−5945.

$[Fe(SEt)_4]^{2-}$, exhibited sample oxidation during irradiation and were not used in this study. PES spectra were simulated to include satellite peaks by utilizing a valence bond configuration interaction (VBCI) model as described later. Full spectroscopic simulations, including VBCI and atomic multiplets, were performed using the TT-Multiplets suite of computer codes, graciously provided by Dr. Frank de Groot.[29] All TT-Multiplet calculations were performed on an SGI Origin server.

Density Functional Calculations. DFT calculations were performed using the commercially available Amsterdam Density Functional (ADF1999 and ADF2000)[30−34] and Gaussian (Gaussian 98)[35] codes. In ADF, the Vosko, Wilk, and Nusair (VWN) local density approximation[36] was supplemented with standard nonlocal corrections from Becke[37] and Perdew[38,39] (BP86). All ADF results were obtained using a triple-ζ STO basis set (Basis IV) for the valence levels of all heavy atoms. Core levels were defined for $n = 1, 2$ for Fe and S and for $n = 1$ for all second-row elements. Complementary calculations using the BP86 functional were performed with Gaussian using a 6-311G(d,p) basis set. Results from the two quantum mechanics codes were similar. Because the available molecular orbital and charge decomposition schemes are different in the two codes, results from both are used in this study. All calculations were performed on either an SGI Origin 2000 8-cpu R10k server running IRIX 6.5.3 or an Intel dual Pentium III Xeon system running RedHat Linux 7.0. Parallelization of ADF and Gaussian was done using built-in PVM and shared-memory architectures, respectively. Details of specific input parameters used for all published calculations are included as Supporting Information.

Results and Analysis

Core Ionization. Core-level Fe $2p_{3/2}$ photoelectron spectroscopic (PES) data for $[FeCl_4]^{2-}$ and $[Fe(SPh)_4]^{2-}$ are given in Figure 1. The data distinctly show an intense main peak (M) and a large satellite (S) feature at higher binding energy. The experimental S-to-M intensity ratios (I_S/I_M) of the two species are very large; I_S/I_M is slightly larger in the tetrathiolate data. For comparison, the data for the ferric species are also given in Figure 1; the satellite features are far weaker in these species. The presence of intense satellite features, as observed in the ferrous species, result from shake-up ionization processes[40−42] that are formally two-electron processes and thus forbidden. These satellite features provide an experimental handle on electronic relaxation, i.e., the change in the electronic wave function that must occur to allow two-electron ionization processes to be observed. A significant body of literature exists on the nature of these satellite peaks. In first-row transition metal complexes, these shake-up states are linked with the presence of charge-transfer (CT) interactions between the metal and its ligands.[40,43−53]

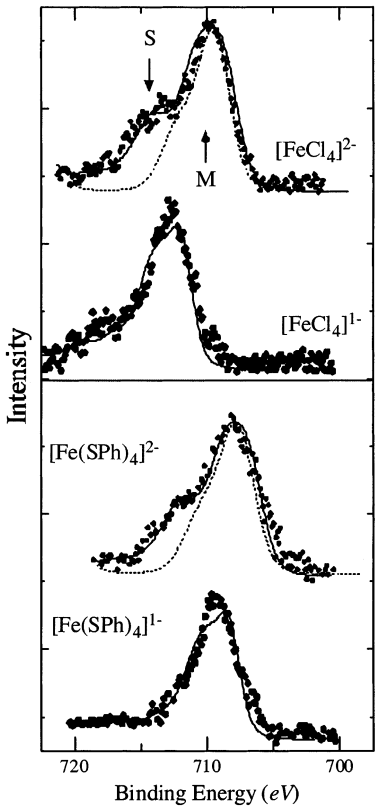

Figure 1. Core-level XPS data for both oxidation states of $[FeCl_4]$ and $[Fe(SR)_4]$. The points are the experimental data, the solid lines represent full simulations of the data including both atomic multiplets and CT states, and the dashed lines correspond to multiplet-only simulations. For both ferrous species, the inclusion of CT states is absolutely necessary for proper simulation of the satellite (S) features at higher binding energy. All simulations are performed using CT parameters listed in Table 1. Detailed input parameters for the TT-Multiplets simulation package are provided as Supporting Information.

A valence bond configuration interaction (VBCI) model provides insight into the ionization and electronic relaxation

(29) For more information on the TT-Multiplets program, see http://www.anorg.chem.uu.nl/PUBLIC/degroot.htm.
(30) Baerends, E. J.; Ellis, D. E.; Ros, P. *Chem. Phys.* **1973**, *2*, 41−51.
(31) Versluis, L.; Ziegler, T. *J. Chem. Phys.* **1988**, *88*, 322−328.
(32) Te Velde, G.; Baerends, E. J. *J. Comput. Phys.* **1992**, *99*, 84−98.
(33) Guerra, C. F.; Snijders, J. G.; Te Velde, G.; Baerends, E. J. *Theor. Chem. Acc.* **1998**, *99*, 391−403.
(34) Te Velde, G.; Bickelhaupt, F. M.; Baerends, E. J.; Fonseca Guerra, C.; van Gisbergen, S. J. A.; Snijders, J. G.; Ziegler, T. *J. Comput. Chem.* **2001**, *22*, 931−967.
(35) Frisch, M. J.; Trucks, G. W.; Schlegel, H. B.; Scuseria, G. E.; Robb, M. A.; Cheeseman, J. R.; Zakrzewski, V. G.; Montgomery, J. A., Jr.; Stratmann, R. E.; Burant, J. C.; Dapprich, S.; Millam, J. M.; Daniels, A. D.; Kudin, K. N.; Strain, M. C.; Farkas, O.; Tomasi, J.; Barone, V.; Cossi, M.; Cammi, R.; Mennucci, B.; Pomelli, C.; Adamo, C.; Clifford, S.; Ochterski, J.; Petersson, G. A.; Ayala, P. Y.; Cui, Q.; Morokuma, K.; Salvador, P.; Dannenberg, J. J.; Malick, D. K.; Rabuck, A. D.; Raghavachari, K.; Foresman, J. B.; Cioslowski, J.; Ortiz, J. V.; Baboul, A. G.; Stefanov, B. B.; Liu, G.; Liashenko, A.; Piskorz, P.; Komaromi, I.; Gomperts, R.; Martin, R. L.; Fox, D. J.; Keith, T.; Al-Laham, M. A.; Peng, C. Y.; Nanayakkara, A.; Challacombe, M.; Gill, P. M. W.; Johnson, B.; Chen, W.; Wong, M. W.; Andres, J. L.; Gonzalez, C.; Head-Gordon, M.; Replogle, E. S.; Pople, J. A. *Gaussian 98*, revision A.1x; Gaussian, Inc.: Pittsburgh, PA, 2001.
(36) Vosko, S. H.; Wilk, L.; Nusair, M. *Can. J. Phys.* **1980**, *58*, 1200−1211.
(37) Becke, A. D. *Phys. Rev. A: Gen. Phys.* **1988**, *38*, 3098−3100.
(38) Perdew, J. P.; Burke, K.; Ernzerhof, M. *ACS Symp. Ser.* **1996**, *629*, 453−462.
(39) Perdew, J. P. *Phys. Rev. B: Condens. Matter* **1986**, *33*, 8822.
(40) Van der Laan, G.; Westra, C.; Haas, C.; Sawatzky, G. A. *Phys. Rev. B: Condens. Matter* **1981**, *23*, 4369−4380.
(41) Zaanen, J.; Westra, C.; Sawatzky, G. A. *Phys. Rev. B: Condens. Matter* **1986**, *33*, 8060−8073.
(42) Didziulis, S. V.; Cohen, S. L.; Gewirth, A. A.; Solomon, E. I. *J. Am. Chem. Soc.* **1988**, *110*, 250−268.
(43) Chandesris, D.; Lecante, J.; Petroff, Y. *J. Appl. Phys.* **1981**, *52*, 1664−1664.
(44) Larsson, S. *Chem. Phys. Lett.* **1975**, *32*, 401−406.
(45) Manson, S. T. *J. Electron Spectrosc. Relat. Phenom.* **1976**, *9*, 21−28.
(46) Robert, T. *Chem. Phys.* **1975**, *8*, 123−135.
(47) Vernon, G. A.; Stucky, G.; Carlson, T. A. *Inorg. Chem.* **1976**, *15*, 278−284.

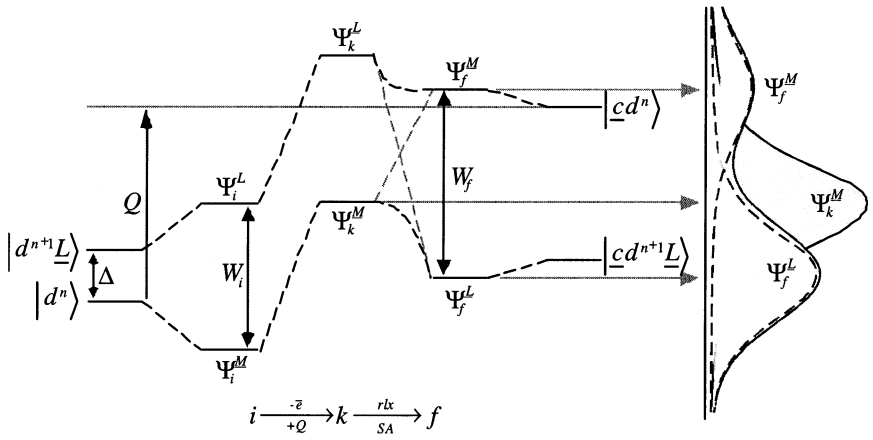

Figure 2. Valence bond configuration interaction (VBCI) model for core ionization of a d^n species. A single CT state is included in this model, although additional states can be added (see text). The Koopmans state ($\Psi_k\underline{^M}$) represents an unrelaxed final state including the effects of Q on the ground-state wave function $\Psi_i\underline{^M}$. Electronic relaxation is defined as the change in charge distribution between $\Psi_k\underline{^M}$ and the lowest-energy final state, $\Psi_f\underline{^L}$.

processes. A representation of the appropriate single-CT state (1CT) VBCI model is given in Figure 2. The model is readily expanded to include more CT states. The 1CT-VBCI model involves mixing of a single LMCT configuration ($|d^{n+1}\underline{L}\rangle$) into the ionic $|d^n\rangle$ ground-state wave function. The resultant ground VBCI states ($\Psi_i\underline{^M}$ and $\Psi_i\underline{^L}$) are defined by the matrix shown in eq 1a. The parameters T and Δ represent the interaction (or covalent mixing) parameter and the splitting of the unmixed ground and CT configurations, respectively. The ground-state covalency is determined from α_i^2, the metal character in the wave function, which equals $\cos^2\theta_i$, where θ_i is defined in eq 1b.[54] The experimental charge-transfer energy ($W_i = E_{CT}$) is also obtained from this treatment, as given in eq 1c. The VBCI approach assumes that overlap between the initial $|d^n\rangle$ and $|d^{n+1}\underline{L}\rangle$ configurations is induced by the off-diagonal term, T. The approach is similar to CNDO-type methods in that overlap of the valence bond configurations is neglected.

$$\begin{bmatrix} 0 & T \\ T & \Delta \end{bmatrix} \quad \begin{aligned} \Psi_i\underline{^M} &= \cos\theta_i|d^n\rangle - \sin\theta_i|d^{n+1}\underline{L}\rangle \\ \Psi_i\underline{^L} &= \sin\theta_i|d^n\rangle + \cos\theta_i|d^{n+1}\underline{L}\rangle \end{aligned} \tag{1a}$$

$$\tan(2\theta_i) = \frac{2T}{\Delta} \tag{1b}$$

$$W_i = E_{CT} = \sqrt{\Delta^2 + 4T^2} \tag{1c}$$

The definition of the final states, $\Psi_f\underline{^M}$ and $\Psi_f\underline{^L}$, is analogous to the above treatment, except that the relative energies of the metal ($|\underline{c}d^n\rangle$) and ligand- ($|\underline{c}d^{n+1}\underline{L}\rangle$) centered states ($\underline{c}$ = core hole on metal) have changed as a result of the differential effect of the 2p−3d hole interaction potential (Q) on the two configurations. Q represents the effect of electron (or hole) repulsion on the two different final-state configurations. The core hole has a destabilizing effect on the $|\underline{c}d^n\rangle$ configuration (Q relative to $|\underline{c}d^{n+1}\underline{L}\rangle$) because there is additional hole−hole repulsion in that configuration. As a result, the energy splitting between the two configurations is now $\Delta - Q$. Notably, when $Q > \Delta$, the order of states inverts in the final state (Figure 2, far right). The VBCI final states and all associated final-state parameters are now defined as in eq 2, with the order of these final states being defined by the sign of $(\Delta - Q)$. As a result of Q, the relative contributions of the two component states change in the final state ($\alpha_f^2 = \sin^2\theta_f \neq \alpha_i^2$); this allows for intensity in the formally forbidden $|d^n\rangle \rightarrow |\underline{c}d^{n+1}\underline{L}\rangle$ two-electron transition.

$$\begin{bmatrix} Q & T \\ T & \Delta \end{bmatrix} \quad \begin{aligned} \Psi_f\underline{^M} &= \cos\theta_f|\underline{c}d^n\rangle - \sin\theta_f|\underline{c}d^{n+1}\underline{L}\rangle \\ \Psi_f\underline{^L} &= \sin\theta_f|\underline{c}d^n\rangle + \cos\theta_f|\underline{c}d^{n+1}\underline{L}\rangle \end{aligned} \tag{2a}$$

$$\tan(2\theta_f) = \frac{2T}{(\Delta - Q)} \tag{2b}$$

$$W_f = \sqrt{(\Delta - Q)^2 + 4T^2} \tag{2c}$$

For the wave functions chosen, the following restrictions are required[40,55]

$$\text{for } \Delta > 0, \quad 0° < \theta_i < 45°$$

$$\text{for } (\Delta - Q) > 0, \quad 0° < \theta_f < 45°$$

and

$$\text{for } (\Delta - Q) < 0, \quad 45° < \theta_f < 90°$$

Within the context of this study, it is useful to define a reference state, termed the Koopmans state, from which electronic relaxation is calculated. This reference state is shown in the central part of Figure 2 and is constructed directly from the initial-state wave functions. The wave

(48) Kato, H.; Ishii, T.; Masuda, S.; Harada, Y.; Miyano, T.; Komeda, T.; Onchi, M.; Sakisaka, Y. *Phys. Rev. B: Condens. Matter* **1985**, *32*, 1992−1996.
(49) Sacher, E. *Phys. Rev. B: Condens. Matter* **1985**, *31*, 4029−4030.
(50) Agren, H.; Carravetta, V. *Int. J. Quantum Chem.* **1992**, *42*, 685−718.
(51) Mayer, B.; Uhlenbrock, S.; Neumann, M. *J. Electron Spectrosc. Relat. Phenom.* **1996**, *81*, 63−67.
(52) Okada, K.; Kotani, A.; Thole, B. T. *J. Electron Spectrosc. Relat. Phenom.* **1992**, *58*, 325−343.
(53) Freund, H. J.; Plummer, E. W.; Salaneck, W. R.; Bigelow, R. W. *J. Chem. Phys.* **1981**, *75*, 4273−4284.
(54) The covalency of the metal−ligand bond reaches a maximum at $\alpha_i^2 = 0.5$.
(55) In certain cases, the value(s) of θ_i and/or θ_f must be adjusted by $\pi/2$ to respect the limits placed herein.

Table 1. VBCI Parameters from Core PES Data[a]

species	$E_b^{Fe\ 2p_{3/2}}$ [b,c]	I_S/I_M[d]	W_f	Δ	T	Q	U[e]	α_i^2
$[FeCl_4]^{2-}$	710.8	0.37	4.5	2.4	1.8	4.5	3.8	0.84
$[FeCl_4]^{1-}$	713.6	0.24	4.8	0.6	1.6	3.8	−	0.63
$[Fe(SR)_4]^{2-}$	709.4	0.41	4.4	1.3	1.6	4.3	3.5	0.76
$[Fe(SR)_4]^{1-}$	709.8	0.23	3.9	0.2	1.3	3.1	−	0.55

[a] All values except for I_S/I_M and α_i^2 are given in electronvolts. For the ferric species, VBCI is solved using W_i(Cl) = 3.2 eV and W_i(SR) = 2.2 eV as input parameters. [b] Reported binding energies are corrected for electronic relaxation as the intensity-weighted average energy of the complete intensity envelope. [c] Experimentally derived energies are accurate to within ~0.3 eV. [d] Intensity ratios were obtained by Gaussian fits of the XPS data; the standard deviation is ~0.04 in all cases. [e] Obtained from simulations of the valence PES data (see text).

functions are frozen such that $\theta_k = \theta_i$ (and thus $\alpha_k^2 = \alpha_i^2$); however, the Koopmans states are affected energetically by Q, according to the amount of $|\underline{c}d^n\rangle$ character in each wave function. The energy destabilization due to Q thus distributes over the two-component Koopmans states as follows

$$E_k\underline{^M} = E_i\underline{^M} + Q(\alpha_i^2)$$
$$E_k\underline{^L} = E_i\underline{^L} + Q(1 - \alpha_i^2) \quad (3)$$

The VBCI model provides the proper tools to define electronic relaxation as a function of changes in the effective charge on the metal on going from the unrelaxed ($\Psi_k\underline{^M}$) to the relaxed ($\Psi_f\underline{^L}$ when $Q > \Delta$) ionized state. The change in charge due to electronic relaxation is thus defined as the change in metal character upon relaxation and is calculated as in eq 4 (specifically for $Q > \Delta$). This model also allows for the calculation of changes in the energies of the states upon relaxation (E_{rlx}); this aspect of the model is developed and used in part 2,[24] which deals with redox thermodynamics.

$$\Delta q_{rlx} = \alpha_k^2 - \alpha_f^2$$
$$= \alpha_i^2 - \alpha_f^2 \quad (4)$$
$$= \cos^2\theta_i - \sin^2\theta_f$$

The relative intensities of the two possible i → f transitions is given experimentally by I_S/I_M (Table 1); it has previously been shown that I_S/I_M is related to the above through eq 5. This equation reflects the application of the sudden approximation to redistribute intensity over the final states.

$$\frac{I_S}{I_M} = \tan^2(\theta_f - \theta_i) \quad (5)$$

Appropriate VBCI parameters can be obtained from the experimental XPS data using the 1CT-VBCI model. The ground-state energy splitting, W_i, is estimated from the onset of charge-transfer absorption in the electronic absorption data, yielding 4.2 and 3.5 eV for the ferrous chloride and thiolate complexes, respectively.[56] Using these values, the 1CT-VBCI model fits to the ferrous data (Figure 1) give the results listed in Table 1.[57] Although the relative satellite energies and intensities for the two ferrous species are reasonably similar, the resultant VBCI parameters are quite different because of the experimental differences in their charge-transfer energies. As a result, the VBCI model allows for the determination of the overall covalency for each system. The XPS results from the 1CT-VBCI model are quite consistent with the results from other experimental and theoretical methods used to calculate the covalency of these systems: $[FeCl_4]^{2-}$ is significantly more ionic than $[Fe(SR)_4]^{2-}$ (see α_i^2 in Table 1).

Table 2. Experimental and Theoretical Values for Electronic Relaxation upon Fe $2p_{3/2}$ Ionization[a]

method	$[FeCl_4]^{2-}$	$[Fe(SR)_4]^{2-}$
1CT-VBCI	−0.63	−0.64
4CT-VBCI	−0.79	−0.82
Hrf-DFT[a]	−1.02	−1.11

[a] Hirshfeld charges from ADF calculations.

The VBCI model, as developed above, does not include some of the complexities of transition metal systems, in particular the atomic multiplets (AMs) that result from high-spin initial states. The basic VBCI approach has been applied together with atomic multiplets in a suite of XAS simulation codes known as TT-Multiplets.[29] These programs create appropriate atomic multiplets for the atomic system of interest and then apply a VBCI perturbation over all component states, in the initial and final states, to obtain a more complete simulation of the spectrum (AM-VBCI).

The two-state fit is extended to include atomic multiplets by using the VBCI parameters in Table 1 to simulate the spectra using the AM-VBCI method. The simulated spectra, shown as the solid black lines in Figure 1, are extremely representative of the data, providing good confidence in the VBCI results obtained from the simpler 1CT-VBCI fits. We note that the inclusion of CT states is needed to simulate the experimental data properly. If simulations are attempted without the higher-lying CT states (dashed lines in Figure 1), the higher-energy satellite features are not well described in the ferrous data. Therefore, the ferrous XPS satellites require the inclusion of formally forbidden CT final states, demonstrating the presence of electronic relaxation. In contrast, the much weaker satellites in the ferric data are reasonably well described by redistribution of intensity into higher-lying atomic multiplets; the importance of CT states (and thus electronic relaxation) in this case is thus much less than in the ferrous species.

The VBCI analysis of the core data for the ferrous species allows us to quantitatively evaluate the changes in the effective charge on the metal due to electronic relaxation (Δq_{rlx}, as summarized in Table 2). From the 1CT-VBCI results, electronic relaxation upon ionization of a core electron is very large in both $[FeCl_4]^{2-}$ and $[Fe(SR)_4]^{2-}$. A concern with the 1CT-VBCI model is its inclusion of only one ligand hole state, which precludes any involvement of higher-order CT processes. Even small contributions from such states could significantly influence Δq_{rlx}, so the 1CT-

(56) Gebhard, M. S.; Koch, S. A.; Millar, M.; Devlin, F. J.; Stephens, P. J.; Solomon, E. I. *J. Am. Chem. Soc.* **1991**, *113*, 1640−1649.

(57) The VBCI parameters provide unique fits except under conditions when either Δ or ($\Delta - Q$) is very near zero. In such cases, the Δ,T solution space is highly correlated and difficult to evaluate.

VBCI model has been systematically extended to include higher-order states. As expected, an increase in the number of CT states leads to a concomitant increase in Δq_{rlx} up to $n = 4$, at which point further changes in Δq_{rlx} become negligible. Results for the 4CT-VBCI analysis are given in Table 2; a net increase of $\sim$0.15−0.20 in Δq_{rlx} is observed relative to the 1CT-VBCI results. Small contributions from higher-order CT states cannot be experimentally verified because of the low resolution of the data. However, the improvement from these higher-order CT states does not change the overall behavior of Δq_{rlx}, and the VBCI analysis provides a simple formula for the inclusion of these unobservable terms. Overall, however, electronic relaxation is found to be very large in both systems, and Δq_{rlx} is consistently observed to be slightly larger for $[Fe(SR)_4]^{2-}$ than for $[FeCl_4]^{2-}$.

Δq_{rlx} can also be evaluated using DFT methods. The unrelaxed ionized state is obtained theoretically by symmetric removal of an Fe 2p electron from the ferrous potential *without* reconverging the potential. The change in charge on the metal ion between the unrelaxed and relaxed final states is analogous to the experimentally derived Δq_{rlx}. Several theoretical methods exist to determine the atomic charge from DFT results; we have chosen to use Hirshfeld charges, which generally yield chemically reasonable results for transition metal systems. The calculated core relaxations are larger than those obtained experimentally (see Table 2) but still support the idea that electronic relaxation is very large in these systems and is somewhat larger in the $[Fe(SR)_4]^{2-}$ complex.

Valence Ionization. Valence photoemission data were obtained for the two ferrous species, both with the $[N(CH_2CH_3)_4]^+$ counterion. Raw data for $[FeCl_4]^{2-}$ at $h\nu = 40$ eV are shown in Figure 3a; the ionization envelope is very broad, a result that is also observed for $[Fe(SR)_4]^{2-}$ (see Figure S1 in the Supporting Information). In comparison to results from a single-crystal VEPES study on $[FeCl_4]^{2-}$ (Figure 3c),[20] the data quality is poor. The problem resides in the nature of the systems under study. Whereas the previous $[FeCl_4]^{2-}$ study was done using the Cs salt,[20] the bulky organic counterion $[N(CH_2CH_3)_4]^+$ is necessary to ensure the stability of the $[Fe(SR)_4]^{2-}$ complex under experimental conditions. Because valence PES data are not site-selective, all of the component atoms of the sample contribute to the overall signal. Therefore, the data contain all of the information relating to ionization of Fe 3d-based MOs, but those ionization peaks are buried amidst other peaks. To resolve Fe 3d-based ionization peaks from the background, the normalized ratio of intensities at two different photon energies, 45 and 25 eV, is used ($\Phi^{45\,eV}_{25\,eV} = I_{45\,eV}/I_{25\,eV}$). Because the atomic photoionization cross section for Fe 3d has a delayed maximum near 45 eV,[58] regions where $\Phi^{45\,eV}_{25\,eV} > 1$ define contributions from the Fe 3d manifold. The resultant Fe 3d contribution spectrum for $[FeCl_4]^{2-}$ is shown in Figure 3b. This spectrum is consistent with that obtained from high-resolution data in that the main (lower-energy) features are at the same binding energies in both spectra.

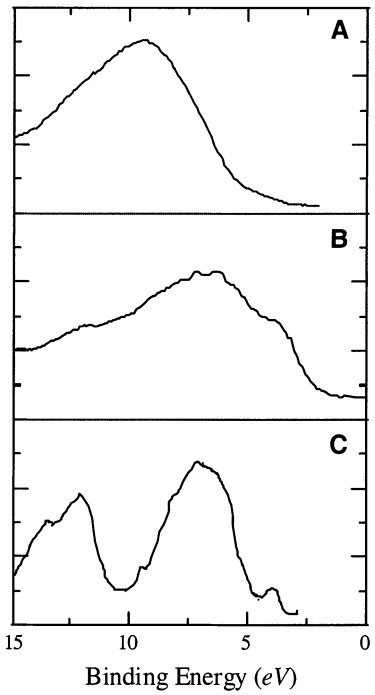

Figure 3. Experimental valence PES data; energy referenced as detailed in the Experimental Section. (A) Raw PES data for $[N(CH_2CH_3)_4]_2[FeCl_4]$ at $h\nu = 40$ eV, (B) $\Phi^{45\,eV}_{25\,eV}$ spectrum obtained from VEPES spectra at $h\nu =$ 45 and 25 eV, (C) high-resolution single-crystal PES data for Cs_2FeCl_4 at $h\nu = 40$ eV. The raw spectrum of the powdered $[N(CH_2CH_3)_4]_2[FeCl_4]$ sample is very broad as a result of ionization peaks from the large organic counterion. The $\Phi^{45\,eV}_{25\,eV}$ spectrum enhances contributions from M3d orbitals. Note the energetic correlations between the features in spectrum B and the raw PES data for Cs_2FeCl_4.

This methodology provides an effective way of extracting useful valence PES information from convoluted data.

The valence $\Phi^{45\,eV}_{25\,eV}$ spectra for both $[FeCl_4]^{2-}$ and $[Fe(SR)_4]^{2-}$ are given in Figure 4. The overall shapes of the spectra are quite similar in that they each contain three regions of intensity: a low-binding-energy shoulder, a major central feature, and a broad envelope of intensity at deeper binding energy. Differences between the data occur in the splitting of the low-energy shoulder from the main peak (larger splitting in $[FeCl_4]^{2-}$) and the overall intensity of the deep-binding-energy envelope (greater intensity in $[Fe(SR)_4]^{2-}$). The energy of the lowest-binding-energy feature is also significantly different (1.4 eV deeper in $[FeCl_4]^{2-}$), an observation that reflects important differences in the redox potentials of these two systems.[24]

Simulated Fe 3d ionization spectra using only atomic multiplets account reasonably well for the low-energy region of the $\Phi^{45\,eV}_{25\,eV}$ spectra but fail in the high-binding-energy region (dashed lines in Figure 4). As for core ionization, the inclusion of CT states (and thus electronic relaxation) is necessary to adequately simulate the full valence spectrum in these complexes. For valence ionization, the VBCI model is essentially identical to that developed for core ionization except that the hole is now created in the Fe 3d manifold. This produces two changes in the analysis. First, the 2p−3d hole interaction is no longer applicable; Q is replaced in the model by an additional 3d−3d interaction potential (U) that destabilizes the $|d^{n-1}\rangle$ state. Second, the creation of a valence

(58) Yeh, J. J.; Lindau, I. *At. Data Nucl. Data Tables* **1985**, *32*, 1−155.

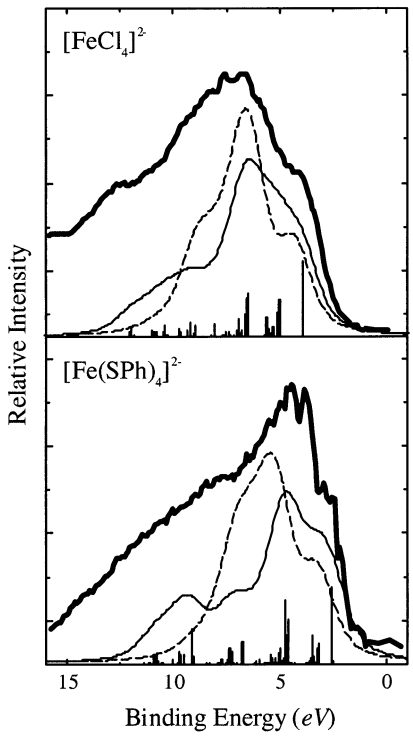

Figure 4. Fe 3d contribution ($\Phi_{25\,eV}^{45\,eV}$) spectra for $[FeCl_4]^{2-}$ and $[Fe(SPh)_4]^{2-}$. The thick solid line (—) is the experimentally obtained $\Phi_{25\,eV}^{45\,eV}$ spectra. The thinner solid line (—) is a complete simulation of the valence ionization spectrum including electronic relaxation. The dashed line (– –) is a simulation of the unrelaxed valence ionization spectrum. The sticks represent the specific component final states of the simulations including electronic relaxation. Simulation parameters are given in Table 1 and as Supporting Information.

hole results in a significant change in the multiplet structure of the final states relative to that of the initial (and Koopmans) states. This is reflected by the significant multiplet structure observed in the low-binding-energy region of the spectra. The implication of this second factor is that atomic multiplets are required in the simulation of valence spectra to obtain reasonable results. For core ionization, simulations are still quite reasonable, even when the 1CT-VBCI model in Figure 2 is used.

To include shake-up satellite features into the simulated valence spectra, the ground-state VBCI parameters obtained from the core ionization data were used because the ground state remained unchanged. The hole interaction parameter was initially assigned as $U = Q$ and then adjusted to find the best simulation of the data. The main effect of modifying U is observed in the energy position of the deep-binding-energy satellites relative to the main peaks. The final simulations (solid lines in Figure 4) were obtained using the values of U given in Table 1. It was found that $U \approx 0.8Q$ gave the best agreement with the experimental data, which is in good agreement with results for other transition metal systems.[59−61]

(59) Atanasov, M.; Potze, R. H.; Sawatzky, G. A. *J. Solid State Chem.* **1995**, *119*, 380−393.
(60) Zaanen, J.; Sawatzky, G. A. *Prog. Theor. Phys. Suppl.* **1990**, 231−270.
(61) Zaanen, J.; Sawatzky, G. A. *J. Solid State Chem.* **1990**, *88*, 8−27.

Table 3. Experimental and Theoretical Values for Δq_{rlx} on Valence Ionization

method		$[FeCl_4]^{2-}$	$[Fe(SR)_4]^{2-}$	$\Delta(\Delta q)$
VBCI	1CT	−0.55	−0.59	0.04
	4CT	−0.69	−0.76	0.08
DFT	AIM[a]	−0.72	−0.76	0.04
	Hrf[b]	−0.58	−0.65	0.07
	Mlk[c]	−0.96	−0.99	0.03

[a] AIM charges from Gaussian 98 calculations. [b] Hirshfeld charges from ADF calculations. [c] Mulliken charges from ADF calculations.

As observed in the core ionization data, the inclusion of CT states allows for satellite intensity at higher binding energies from the main metal ionization peaks. For the valence data, the correlation between the simulations and the $\Phi_{25\,eV}^{45\,eV}$ spectra cannot be exact, as the $\Phi_{25\,eV}^{45\,eV}$ spectra are not true ionization spectra and provide only qualitative information with regard to spectroscopic intensities. Even so, the energy correlations between the data and simulations are reasonable. Although the presence of deeper-binding-energy peaks in the data might also be ascribed to covalent mixing, an earlier high-resolution study of $[FeCl_4]^{2-/1-}$ has shown that the ligand-based orbitals are at lower binding energy than the intensity that results from the satellites.[20] This result will also hold for the tetrathiolate because the ligand orbitals will be at even lower binding energies. Additionally, the applicability of the sudden approximation for these valence ionization processes has also been verified for $[FeCl_4]^{2-}$ and should also hold for $[Fe(SR)_4]^{2-}$. As for core ionization (vide supra), we can calculate Δq_{rlx} for both $[FeCl_4]^{2-}$ and $[Fe(SR)_4]^{2-}$; the results are given in Table 3 for the 1CT-VBCI and 4CT-VBCI analyses. The additional CT states again increase the calculated Δq_{rlx} values but do not change their relative magnitudes. The values of Δq_{rlx} for the valence ionization process are smaller than those for core ionization, but they are still large for both complexes. The differences between $[FeCl_4]^{2-}$ and $[Fe(SR)_4]^{2-}$ [see $\Delta(\Delta q_{rlx})$ in Table 3] are somewhat more pronounced for valence ionization; electronic relaxation upon valence ionization is larger in the tetrathiolate complex.

Electronic relaxation for valence ionization can also be investigated using DFT methods, as was done for core ionization. Results for valence Δq_{rlx} values were calculated using both Hirshfeld and Atoms in Molecules (AIM) charge decomposition schemes and are given in Table 3. The DFT values for Δq_{rlx}, particularly those from AIM, are in good agreement with results obtained from experimental data. Electronic relaxation is clearly quite substantial for the valence ionizations of $[FeCl_4]^{2-}$ and $[Fe(SR)_4]^{2-}$, and Δq_{rlx} is somewhat larger for the tetrathiolate. The Mulliken charge decomposition scheme overestimates the amount of electronic relaxation that occurs in valence ionization (see Table 3), but it provides an opportunity to investigate the origin of electronic relaxation with respect to changes in MO structure upon ionization of the redox-active molecular orbital (RAMO). Mulliken analyses of the electron density distribution changes in $[FeX_4]^{2-}$ upon electronic relaxation are given in Tables 4 and 5. Although there are quantitative differences in the relaxation processes of $[FeCl_4]^{2-}$ and $[Fe(SR)_4]^{2-}$, their

Table 4. Symmetry-Based MO Description of Electronic Relaxation upon Oxidation of $[FeCl_4]^{2-}$

			Δq_{rlx}				
			a_1 $3d_{z^2}$	b_1[b] $3d_{x^2-y^2}$	b_2 $3d_{xy}$	e $3d_{xz,yz}$	total Δq_{rlx}
Fe	α	s/p	−0.048		−0.016	−0.034	−0.13
		d	0.006	−0.011	−0.013	−0.009	−0.04
		tot	−0.041	−0.011	−0.029	−0.043	−0.17
	β	s/p	−0.058		−0.029	−0.034	−0.16
		d	−0.110	−0.099	−0.168	−0.131	−0.64
		tot	−0.168	−0.099	−0.197	−0.165	−0.80
	total		−0.209	−0.110	−0.226	−0.208	−0.97
Cl	α	s/d	−0.004	0.005	0.003	0.004	0.01
		p	0.051	0.006	0.026	0.038	0.16
		tot	0.047	0.011	0.030	0.042	0.17
	β	s/d	−0.001	−0.002	−0.002	−0.001	0.01
		p	0.173	0.101	0.199	0.165	0.80
		tot	0.172	0.099	0.197	0.164	0.81
	total		0.219	0.110	0.227	0.206	0.96

[a] Values are differences between the total Mulliken populations of the spin density in specified symmetry blocks between the relaxed ferric final state and the unrelaxed Koopmans state. [b] The b_1 symmetry block includes the redox-active molecular orbital, from which the valence electron is removed to create the Koopmans state.

Table 5. Symmetry-Based MO Description of Electronic Relaxation upon Oxidation of $[Fe(SCH_3)_4]^{2-}$

			Δq_{rlx}					
			a_1[b] $3d_{z^2}$	a_2[c] −	b_1 $3d_{x^2-y^2}$	b_2 $3d_{xy}$	e $3d_{xz,yz}$	total Δq_{rlx}
Fe	α	s/p	−0.04			−0.05	−0.02	−0.13
		d	−0.04		−0.01	−0.02	−0.01	−0.09
		tot	−0.08		−0.01	−0.07	−0.03	−0.22
	β	s/p	−0.04			−0.02	−0.03	−0.12
		d	−0.06		−0.14	−0.09	−0.18	−0.63
		tot	−0.10		−0.14	−0.11	−0.21	−0.77
	total		−0.18	0.00	−0.15	−0.18	−0.24	−0.99
SCH_3	α	S	0.04	−0.03		0.04	−0.01	0.03
		R	0.04	0.03		0.01	0.06	0.20
		tot	0.08	0.00	0.00	0.05	0.05	0.23
	β	S	0.05	−0.02	0.09	0.07	0.15	0.49
		R	0.05	0.02	0.03	0.04	0.05	0.24
		tot	0.10	0.00	0.12	0.11	0.20	0.73
	total		0.18	0.00	0.12	0.16	0.25	0.96

[a] Values are differences between the total Mulliken populations of the spin density in specified symmetry blocks between the relaxed ferric final state and the unrelaxed Koopmans state. [b] The a_1 symmetry block includes the redox-active molecular orbital, from which the valence electron is removed to create the Koopmans state. [c] The a_2 symmetry block contains no valence Fe character and corresponds to ligand nonbonding interactions.

overall behaviors are very similar, and the mechanisms of electronic relaxation are the same. The electron density change is divided in each case into its component spin and symmetry blocks. For D_{2d} $[FeCl_4]^{2-}$, the RAMO ($3d_{x^2-y^2}$) has b_1 symmetry, whereas D_{2d} $[Fe(SCH_3)_4]^{2-}$ RAMO ($3d_{z^2}$) has a_1 symmetry.[62] In both cases, the *active* symmetry block (the β-spin symmetry block that contains the RAMO) responds to ionization by a modest transfer of electron density from the ligand to the metal. The charge relaxation from this active block of MOs ($\Delta q_{rlx}^{active} \approx -0.1$ in both) accounts for only a small portion of the total Δq_{rlx}. The other minority (β) spin symmetry blocks that involve Fe−L bonding contribute far more strongly to Δq_{rlx}. As a whole, changes in these *passive* β-spin levels account for ∼80% of the electronic relaxation. This corresponds to a systematic increase in the mixing between the Fe 3d and L 3p manifolds. The covalency of the Fe−L bonds increases such that the ligand contribution to each of the five empty Fe 3d orbitals increases by ∼0.10−0.15. Changes in the majority (α) spin blocks contribute only slightly to Δq_{rlx} (∼10%). In these blocks, specific changes in covalency due to mixing of the Fe 3d and L 3p manifolds cannot directly change the charge distribution because both manifolds are full. For the α-spin blocks, ligand-to-metal charge transfer occurs by increasing the amount of Fe 4s/p character in the final states. This is consistent with Fe K-edge XAS data, which indicate a much greater degree of Fe 4p mixing in $[FeCl_4]^{1-}$ relative to $[FeCl_4]^{2-}$.[63]

Discussion

Electronic relaxation is a concept that is generally neglected in the evaluation and description of redox processes in chemical species. This study of the electronic structure of $[FeX_4]^{2-}$ (X = Cl, SR) complexes and their responses to ionization allows us to evaluate electronic relaxation quantitatively. Our experimental data, corroborated by DFT results, demonstrate the dramatic influence of electronic relaxation on the overall electronic structure description of $[FeX_4]^{2-}$ complexes on ionization. This study further quantifies electronic relaxation as a function of changes in the effective charge at the central metal ion (Δq_{rlx}) in response to ionization. Valence ionization of $[FeCl_4]^{2-}$ ($\Delta q_{rlx}^{avg} = -0.65$) and $[Fe(SR)_4]^{2-}$ ($\Delta q_{rlx}^{avg} = -0.70$) results in dramatic charge donation from the ligands to compensate for the creation of a valence hole at the metal center. The origin of this ligand-to-metal charge transfer has been determined by DFT methods. Most generally, we note the direct correlation of an experimental observable, the intensity of CT satellite features in valence and core PES data, to the magnitude of electronic relaxation on oxidation.

Within this study, two methods have been used to address the mechanisms that allow electronic relaxation. Mulliken partitioning of changes in DFT-calculated electron densities upon ionization provides important insight into the nature of electronic relaxation. The results clearly demonstrate that a simple one-electron representation of the ionization process is misleading. The description of the RAMO, from which the electron is removed, is inconsistent with the electron density changes that are observed upon ionization. Changes in the RAMO account for only a small percentage of the observed electronic relaxation. The response of passive

(62) The nature of the RAMO in $[Fe(SR)_4]$ complexes is highly dependent on the orientation of the thiolate ligands (see ref 42 for details). In this particular case, the $3d_{z^2}$ orbital is lowest in energy.

(63) Westre, T. E.; Kennepohl, P.; DeWitt, J. G.; Hedman, B.; Hodgson, K. O.; Solomon, E. I. *J. Am. Chem. Soc.* **1997**, *119*, 6297−6314.

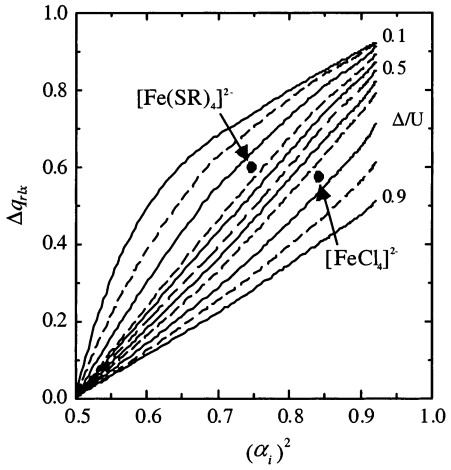

Figure 5. Relationship between the ground-state α_i^2 and Δq_{rlx}. The lines are given for specific values of Δ/U as calculated from the VBCI model developed in the text. For a fixed Δ/U value, increasing covalency (decreasing α_i^2) results in a decrease in Δq_{rlx}. However, decreasing Δ/U increases Δq_{rlx}. The experimentally derived values for $[FeCl_4]^{2-}$ and $[Fe(SPh)_4]^{2-}$ are shown in the figure.

electrons involved in specific Fe−L bonding interactions plays a critical role in stabilizing the ionized final state. Good mechanisms for LMCT include the dominant Fe 3d−L 3p interactions as well as some contribution from Fe 4s/p−L 3p interactions, as evidenced by relaxation contributions from α-spin MOs. These DFT results underscore the important contributions from passive electrons in stabilizing the oxidized site.

The VBCI model provides further insight into the factors that affect valence electronic relaxation. It is tempting to suggest that a larger ground-state covalency (i.e., a lower α_i^2) will limit electronic relaxation. Although this is generally true, it is complicated by the fact that several competing factors contribute to the dependence of Δq_{rlx} on α_i^2, as shown in Figure 5. Within the VBCI model, α_i^2 is defined by T and Δ. The effect of the mixing parameter, T, essentially parallels the behavior of α_i^2; increasing T decreases α_i^2 and Δq_{rlx}. This result is reasonable in that an already highly covalent system has fewer options in allowing for additional LMCT upon oxidation. The effect of Δ is far more complex and cannot be discussed independently of U given that both parameters together determine the relative energy splittings of the initial and final states (see Figure 2). We find that, as a general rule, decreasing Δ/U serves to increase Δq_{rlx} (see Figure 5); therefore, increasing U and/or decreasing Δ will increase Δq_{rlx}. When comparing $[FeCl_4]^{2-}$ and $[Fe(SR)_4]^{2-}$, we find that Δq_{rlx} of the latter is greater than that of the former despite its more highly covalent ground state. The greater Δq_{rlx} during ionization of $[Fe(SR)_4]^{2-}$ occurs because of its significantly lower Δ value as compared to $[FeCl_4]^{2-}$ (the magnitude of U is quite similar). Physically, the available CT states necessary for electronic relaxation are much lower in energy in the tetrathiolate than in the comparable chloride complex, thus allowing for increased LMCT upon ionization.

The above analysis is based on the 1CT-VBCI model and therefore cannot include the potential influence of other CT states. Within the context of our study of specific $[FeX_4]^{2-}$ complexes with reasonably similar initial-state descriptions, the model is reasonable in providing a qualitative understanding of the factors affecting the phenomenon, as well as a semiquantitative method of obtaining experimentally derived estimates of electronic relaxation. We note that increasing the sophistication of the model by adding additional CT states and atomic multiplet effects (vide supra) does not change the fundamental results: Δq_{rlx} is large in both systems, with a higher value for the tetrathiolate complex. DFT results provide similar insights into the process, although the results are too large for the core ionization process. Discrepancies between the experimental and theoretical results are mostly attributed to the difficulty in theoretically defining atomic charges in covalent molecular systems.

Previous theoretical work has suggested that $[FeX_4]^{2-,1-}$ redox couples are best described as *ligand-based* redox processes, in contrast with the viewpoint generally accepted by experimentalists that such processes are essentially *metal-based*. The extent of electronic relaxation in these systems, dominated by the influence of passive electrons, provides the proper context for these differing descriptions of the redox process. The dramatic influence of electronic relaxation creates a situation wherein the overall oxidation process involves the loss of more electron density from the ligands than the central metal ion. In fact, we have found that the effective charge at the metal site (Δq_{redox}) changes only very little upon oxidation of these complexes.[25,64] The change in charge on the metal during redox is only $0.1\bar{e}$ for $[Fe(SR)_4]^{2-,1-}$, even though the electron is removed from a mostly metal-based molecular orbital.[65] This result arises directly from the massive ligand-to-metal charge transfer in response to ionization of the (metal-based) redox-active molecular orbital. Importantly, electronic relaxation redistributes electron density back to the metal *over all M−L bonding interactions*, with a dominant contribution from passive electrons. The distribution of the LMCT relaxation over multiple MOs creates a relaxed final (oxidized) state that is best described as a highly covalent $3d^5$ system. The sum of the changes over all M−L bonding interactions causes the overall process to be ligand-based, even though the ionized electron is removed from a metal-based MO.

Final Remarks

This study provides a foundation for the investigation of electronic structure contributions to the redox properties of $[FeX_4]^{2-,1-}$ active sites. We have provided experimental and theoretical data that demonstrate the dramatic influence of electronic relaxation on the ionization processes of the reduced $[FeX_4]^{2-}$ species. In the following two complementary studies, we use the results of this study as the starting point for the investigation of electronic structure contributions to the thermodynamic[24] and kinetic properties[25] of

(64) Small changes in the effective charge of transition metal complexes have been noted previously (see: Bagus, P. S.; Walgren, U. I.; Almlof, J. *J. Chem. Phys.* **1976**, *64*, 2324−2334), but the nature of this effect has not been determined experimentally.

(65) Kennepohl, P.; Solomon, E. I. *J. Am. Chem. Soc.*, manuscript submitted.

$[Fe(SR)_4]^{2-,1-}$ electron-transfer sites. In these studies, the greater electronic relaxation in $[Fe(SR)_4]^{2-,1-}$ relative to $[FeCl_4]^{2-,1-}$ is found to contribute strongly to differences in their redox potentials and electron-transfer rates. Elsewhere, we have also detailed the importance of these effects on the redox properties of rubredoxins, an important class of ET proteins.[65] Electronic relaxation in $[Fe(SR)_4]^{2-,1-}$ and related redox couples is thus found to be of direct importance in defining the ability of such redox centers to function as efficient electron-transfer active sites.

Acknowledgment. Financial support for this research was provided by the National Research Foundation (NSF CHE-9980549). Valence PES data were obtained at the Stanford Synchrotron Radiation Laboratory (SSRL). SSRL is funded by the U.S. Department of Energy, Office of Basic Energy Sciences. Partial financial support was provided to P.K. from SSRL. Additional financial support for P.K. was provided by the Natural Sciences and Engineering Research Council of Canada (NSERC/CRSNG) in the form of a 1967 Science & Engineering Graduate Scholarship. Dr. Frank De Groot (Universiteit Utrecht) provided the TT-Multiplets suite of programs and assisted in its utilization. Some of the core PES data were obtained on the VG Instruments M-Probe at the Beckman Institute (California Institute of Technology) with generous support and assistance from Prof. Nathan Lewis and Dr. Michael Freund. Technical assistance on the M-Probe was provided by Elizabeth Mayo at Caltech.

Supporting Information Available: Input files and structural information for all DFT results used in this paper. Figure showing raw valence PES data for $[N(Et)_4]_2[Fe(SPh)_4]$. This material is available free of charge via the Internet at http://pubs.acs.org.

IC020330F